A NON-OSCILLATORY KINETIC SCHEME FOR MULTI-COMPONENT FLOWS WITH THE EQUATION OF STATE FOR A STIFFENED GAS*

Yibing Chen　　and　　Song Jiang

Institute of Applied Physics and Computational Mathematics P.O. Box 8009, Beijing 100088, China
E-mail: chen_yibing@iapcm.ac.cn　　jiang@iapcm.ac.cn

Abstract

We extend the traditional kinetic scheme for ideal gases to the Euler equations with the equation of state for a multi-component stiffened gas. Based on a careful analysis of the oscillation mechanism of the traditional kinetic scheme across contact discontinuities, we propose a new non-oscillatory kinetic (NOK) scheme for multi-component stiffened gases. The basic idea in the construction is to use a flux splitting technique to construct numerical fluxes which do not depend on the concrete form of the equilibrium state. The new scheme can not only can avoid spurious oscillations of the pressure and velocity near a material interface which are observed in the traditional kinetic schemes such as the kinetic flux vector splitting (KFVS) and BGK schemes, but also can deal with the stiffened gas equation of state. Moreover, we also carry out a careful analysis on the consistency condition, truncation error and positivity of the NOK scheme. A number of 1D and 2D numerical tests are presented which demonstrate the accuracy and robustness of the new scheme in the simulation of problems with smooth, weak and strong shock wave regions.

Mathematics subject classification: 65M06, 82C40, 35L64, 76N10.
Key words: Kinetic scheme, Non-oscillation, Multi-component, Stiffened gases.

1. Introduction

In the past years, the development of numerical methods for compressible multi-component flows with general equations of state has attracted much attention. When a compressible inviscid flow includes several components, the flow can be modeled by the so-call extended Euler equations. The extended Euler equations consist of the traditional compressible Euler equations and the species equations which describe the conservation of the species. The extended Euler equations are no longer strictly hyperbolic, but a weakly hyperbolic system. And traditional conservative schemes, for example, the high order and high resolution schemes such as MUSCL [35], TVD [12], ENO [13] which work well in the numerical simulation of single component flows, may not give satisfactory numerical results for the extended Euler equations. In fact, it had been demonstrated in both theory and numerical tests that traditional conservative schemes could produce spurious pressure oscillations near material interfaces when they are used to solve the extended Euler equations [20].

Great efforts have been made to circumvent this difficulty in the past two decades [1,11,15, 20,21,30]. One of the popular methods is quasi-conservative algorithm proposed by Abgrall [1] and then generalized by Shyue [30–32]. Instead of the full conservative formulation, the quasi-conservative algorithm uses a quasi-conservative formulation of the extended Euler equations to

ensure a consistent approximation of the energy equation near a material interface. A Godunov-type method with a generalized version of Roe's approximate Riemann solver was utilized to construct the quasi-conservative algorithm. The algorithm works well in the regions of smooth flows and moderate-strength shock waves. However, it was suggested by Shyue that it would be better to select the exact Riemann solver to deal with strong shock waves [30]. As is well-known, it is complex and expensive to construct the exact Riemann solver for general equations of state (EOS).

Instead, much efforts have been made in constructing Riemann-solver-free schemes of high-order and high-resolution, and one of such schemes is the gas kinetic scheme (GKS). Different from traditional Godunov-type methods, the GKS is based on the Boltzmann equation which provides more information on the flow and can describe the flux function of the governing equations by particle collision of the transport process. Once the particle distribution function on a cell interface is obtained, the numerical flux can be calculated directly.

In the last decades, significant progress has been achieved in the study of the GKS, see e.g., [6, 8, 9, 18, 19, 23, 34, 40], [24]– [28], [36]– [39]. The kinetic flux vector splitting scheme (KFVS) and the BGK scheme are among the GKS. A KFVS scheme solves the collisionless Boltzmann equation while a BGK scheme solves the Bhatnagar-Gross-Krook (BGK) model which is the most famous one of the simplified models of the Boltzmann equation. Besides, the so-called kinetically consistent difference scheme (KCDS) was proposed in 1980s by Russian mathematicians which in fact coincides with the KFVS (cf. [3]). Nowadays, the KCDS has been used in solving gas dynamical and quasi-gas dynamical problems, such as complex flows of viscous heat-conducting gases [10] and binary non-reacting gas mixture [9]. Also, the adaption of the KCDS to the architecture of multiprocessor systems with distributed memory was discussed in [3, Chapter IV].

In the recent years, the GKS has been used to simulate multi-component flows. The early attempt was made by Xu in 1997 [36], and then by Lian [22], Tang and Wu [33]. Further development can be found in [16, 17]. All the constructed schemes in [16, 17, 22, 33, 36] are based on the fully conservative formulation and work well when the difference of physical characters between two species is not too large. Consequently, these schemes cannot be applied to wider range of applications, in particular, to the simulation of flows with general EOS. In fact, two difficulties have to be overcome before the GKS can be widely used to simulate multi-components flow with general EOS. The first difficulty, as aforementioned, is that conservative schemes will produce pressure oscillations near a material interface. Such oscillations are also present in the conservative GKS. Furthermore, as pointed out by the authors [2], the traditional GKS will produce the pressure and velocity oscillations near contact discontinuities even in case of single material fluids. The second one is that the traditional GKS, which is based on the theory of rarefied gas dynamics, may not be extended directly to more general materials such as liquids and solids. In fact, it is difficult to construct a (universal) equilibrium state and a single kinetic transport equation to exactly recover the compressible Euler equations with general EOS of real materials.

The mechanism inducing the first difficulty was carefully analyzed by the authors of this paper [2] in the case of ideal gases, and a so-called consistent condition for constructing numerical fluxes was proposed to modify the traditional KFVS scheme, so that the oscillations across a contact discontinuity can be diminished. Consequently, a new modified scheme – MKFVS scheme was proposed to solve the quasi-conservative extended Euler equations. The new scheme eliminates spurious oscillations near a contact discontinuity in the case of both single and multi

materials. The second difficulty can be illuminated by the idea of flux splitting method used by Xu in the solution of the MHD equations [37], where Xu obtained the relationship between the particle distribution function and all the flux functions of the (macro) governing equations and the relationship is in fact independent of the form of EOS. Although Xu still dealt with ideal gases in [37], the idea may be adapted to treat more general materials.

In this article, adapting the ideas from [37] and [2], we will construct a robust gas kinetic scheme to simulate multi-component flows with general EOS.

This article is organized as follows. In Section 2, adapting the idea in [37], we recall the kinetic scheme by a flux splitting technique. In Section 3, we will analyze the mechanism inducing oscillations of the traditional GKS. In Section 4, after having carefully analyzed the behavior of the GKS, we will propose a new non-oscillatory kinetic scheme for multi-component flows with general EOS, while in Section 5, a number of numerical tests are presented which demonstrate the analysis in Section 4. Finally, conclusions are given in Section 6.

2. Kinetic Flux Splitting Method for the Euler Equations

In this section, based on a flux splitting technique, we follow the idea in [37] to recall the kinetic scheme for ideal gases. Then, in the next section, we will extend the scheme to fluids with more general equations of state. In the 1-D case, the Euler equations can be written as

$$\frac{\partial \vec{W}}{\partial t} + \frac{\partial F(\vec{W})}{\partial x} = 0, \tag{2.1}$$

where

$$\vec{W} = (\rho, \rho U, \rho E)^T,$$
$$F(\vec{W}) = (\rho U, \rho U^2 + P, \rho E U + P U)^T,$$

where ρ, U, P, $E = \frac{1}{2}U + e$ and e are the density, velocity, pressure, total energy and internal energy, respectively. For a ideal gas, P has the form:

$$P = (\gamma - 1)\rho e = (\gamma - 1)(\rho E - \frac{1}{2}\rho U^2), \tag{2.2}$$

where γ is the ratio of specific heats.

Suppose that the computational cells are uniform with the cell size Δx, and the time step is denoted by Δt. Then, the standard finite volume method (FVM) for the Euler equations can be written as

$$\vec{W}_j^{n+1} = \vec{W}_j^n - \sigma(F_{j+\frac{1}{2}} - F_{j-\frac{1}{2}}),$$

where $\sigma = \Delta t/\Delta x$, $F_{j\pm 1/2}$ are the numerical fluxes. A gas kinetic scheme is namely to construct $F_{j\pm 1/2}$ by using Boltzmann-type equations, such as the BGK-model.

From the statistical physics point of view, particles in each computational cell can be supposed as in local equilibrium state. Thus, the particles can be mostly described by the Maxwellian distribution function:

$$g = \rho \left(\frac{\lambda}{\pi}\right)^{1/2} e^{-\lambda(u-U)^2},$$

where U is the fluid velocity, u is the particle velocity, and $\lambda = \frac{m}{2kT}$, m is the molecular mass, k is the Boltzmann constant, and T is the temperature. The particle velocity varies in $(-\infty, \infty)$

and all the particles in a computational cell can be split into two parts: the particles with positive velocity $u > 0$ and the particles with negative velocity $u < 0$. Therefore, the particles with $u > 0$ on the left-hand side of a cell interface and the particles with $u < 0$ on the right-hand side may run across the cell interface. Thus, the transport of the conservative quantities on the cell interface will depend on the collision between the particles across the interface. Before splitting the particles in cells, we denote for simplicity,

$$\tilde{g} = \left(\frac{\lambda}{\pi}\right)^{1/2} e^{-\lambda(u-U)^2}, \quad \langle \cdots \rangle = \int_{-\infty}^{+\infty} (\cdots)\tilde{g}du, \tag{2.3a}$$

$$\langle \cdots \rangle_+ = \int_{0}^{+\infty} (\cdots)\tilde{g}du, \quad \langle \cdots \rangle_- = \int_{-\infty}^{0} (\cdots)\tilde{g}du. \tag{2.3b}$$

Then, we have

$$\langle u^n \rangle = \int_{-\infty}^{+\infty} u^n \tilde{g}du,$$

and it is easy to see that

$$\langle u^{n+2} \rangle = U \langle u^{n+1} \rangle + \frac{n+1}{2\lambda} \langle u^n \rangle, \quad n = 0, 1, \cdots \tag{2.4a}$$

$$\langle u^0 \rangle = 1, \quad \langle u^1 \rangle = U. \tag{2.4b}$$

Splitting the particles into two parts (the one with $u > 0$ and another with $u < 0$) gives

$$\langle u^0 \rangle_+ = \frac{1}{2}\text{erfc}(-\sqrt{\lambda}U), \qquad \langle u^0 \rangle_- = \frac{1}{2}\text{erfc}(\sqrt{\lambda}U),$$

$$\langle u^1 \rangle_+ = U\langle u^0 \rangle_+ + \frac{e^{-\lambda U^2}}{\sqrt{\pi\lambda}}, \quad \langle u^1 \rangle_- = U\langle u^0 \rangle_- - \frac{e^{-\lambda U^2}}{\sqrt{\pi\lambda}},$$

where erfc is the complementary error function. First, let us split the density into

$$\rho^+ = \int_{0}^{+\infty} \rho\tilde{g}du = \rho\langle u^0 \rangle_+, \quad \rho^- = \int_{-\infty}^{0} \rho\tilde{g}du = \rho\langle u^0 \rangle_-.$$

Similar, any quantity Z, which is independent of the velocity U, can be split into

$$Z^+ = Z \int_{0}^{+\infty} \tilde{g}du = Z\langle u^0 \rangle_+, \quad Z^- = Z \int_{-\infty}^{0} \tilde{g}du = Z\langle u^0 \rangle_-;$$

for example,

$$P = P^+ + P^- = P\langle u^0 \rangle_+ + P\langle u^0 \rangle_-.$$

Then, we split the momentum into

$$\rho U = \int_{-\infty}^{\infty} ugdu = \int_{-\infty}^{0} ugdu + \int_{0}^{\infty} ugdu = \rho\langle u^1 \rangle_+ + \rho\langle u^1 \rangle_-,$$

which gives,

$$\rho U = (\rho U)^+ + (\rho U)^-,$$

where

$$(\rho U)^+ = \rho\langle u^1 \rangle_+, \quad (\rho U)^- = \rho\langle u^1 \rangle_-.$$

Similarly, the kinetic energy is split into

$$(\rho U^2)^+ = \rho U \langle u^1 \rangle_+, \quad (\rho U^2)^- = \rho U \langle u^1 \rangle_-.$$

Next, the total energy ρE can be split into $(\rho E)^+$ and $(\rho E)^-$ with

$$(\rho E)^+ = \int_0^{+\infty} \frac{1}{2} u^2 g \, du = \frac{1}{2} \langle u^2 \rangle_+ = \frac{1}{2} \rho U \langle u^1 \rangle_+ + \frac{\rho}{4\lambda} \langle u^0 \rangle_+$$

$$= \frac{1}{2} \rho U \langle u^1 \rangle_+ + \rho e \langle u^0 \rangle_+,$$

$$(\rho E)^- = \int_{-\infty}^0 \frac{1}{2} u^2 g \, du = \frac{1}{2} \langle u^2 \rangle_- = \frac{1}{2} \rho U \langle u^1 \rangle_- + \frac{\rho}{4\lambda} \langle u^0 \rangle_-$$

$$= \frac{1}{2} \rho U \langle u^1 \rangle_- + \rho e \langle u^0 \rangle_-.$$

According to the analysis in [36], we have used $\rho e = \rho/(4\lambda)$. Thus, the kinetic energy and internal energy can be split into

$$\frac{1}{2} \rho U^2 = (\frac{1}{2} \rho U^2)^+ + (\frac{1}{2} \rho U^2)^- = \frac{1}{2} \rho U \langle u^1 \rangle_+ + \frac{1}{2} \rho U \langle u^1 \rangle_-,$$

$$\rho e = (\rho e)^+ + (\rho e)^- = \rho e \langle u^0 \rangle_+ + \rho e \langle u^0 \rangle_-.$$

Finally, we consider the energy transport term. In view of

$$\int_0^{+\infty} \frac{1}{2} u^3 \, du = \frac{1}{2} \langle u^3 \rangle_+ = (\frac{1}{2} \rho U^2 + \rho e) \langle u^1 \rangle_+ + \frac{1}{2} U P \langle u^0 \rangle_+ + \frac{1}{2} P \langle u^1 \rangle_+$$

$$= \rho E \langle u^1 \rangle_+ + \frac{1}{2} U P \langle u^0 \rangle_+ + \frac{1}{2} P \langle u^1 \rangle_+,$$

$$\int_0^{+\infty} \frac{1}{2} u^3 \, du = \frac{1}{2} \langle u^3 \rangle_+ = (\frac{1}{2} \rho U^2 + \rho e) \langle u^1 \rangle_- + \frac{1}{2} U P \langle u^0 \rangle_- + \frac{1}{2} P \langle u^1 \rangle$$

$$= \rho E \langle u^1 \rangle_- + \frac{1}{2} U P \langle u^0 \rangle_- + \frac{1}{2} P \langle u^1 \rangle_-,$$

we see that

$$(\rho E U) = (\rho E U)^+ + (\rho E U)^- = \rho E \langle u^1 \rangle_+ + \rho E \langle u^1 \rangle_-,$$

$$P U = \frac{1}{2} U P \langle u^0 \rangle_+ + \frac{1}{2} P \langle u^1 \rangle_+ + \frac{1}{2} U P \langle u^0 \rangle_- + \frac{1}{2} P \langle u^1 \rangle_-.$$

Considering the above splitting and according to the particle velocity, we split the the flux functions of the Euler equations into two parts:

$$\begin{pmatrix} \rho U \\ \rho U^2 + P \\ \rho E U + P U \end{pmatrix} = \begin{pmatrix} \rho U \\ \rho U^2 + P \\ \rho E U + P U \end{pmatrix}^+ + \begin{pmatrix} \rho U \\ \rho U^2 + P \\ \rho E U + P U \end{pmatrix}^- =: F^+ + F^-,$$

where

$$F^+ = \begin{pmatrix} \rho \\ \rho U \\ \rho E \end{pmatrix} \langle u^1 \rangle_+ + \begin{pmatrix} 0 \\ P \langle u^0 \rangle_+ \\ \frac{1}{2} P \langle u^1 \rangle_+ + \frac{1}{2} P U \langle u^0 \rangle_+ \end{pmatrix},$$

$$F^- = \begin{pmatrix} \rho \\ \rho U \\ \rho E \end{pmatrix} \langle u^1 \rangle_- + \begin{pmatrix} 0 \\ P \langle u^0 \rangle_- \\ \frac{1}{2} P \langle u^1 \rangle_- + \frac{1}{2} P U \langle u^0 \rangle_- \end{pmatrix}.$$

For a KFVS scheme, the numerical flux can be simply expressed as

$$F_{j+\frac{1}{2}}^{K} = F_j^+ + F_{j+1}^-, \qquad (2.5)$$

while for a BGK scheme, because the equilibrium state can be calculated by

$$\begin{pmatrix} \bar{\rho} \\ \bar{\rho}\bar{U} \\ \bar{\rho}\bar{E} \end{pmatrix}_{j+\frac{1}{2}} = \begin{pmatrix} \rho \\ \rho U \\ \rho E \end{pmatrix}_j^+ + \begin{pmatrix} \rho \\ \rho U \\ \rho E \end{pmatrix}_{j+1}^-,$$

the corresponding numerical flux can be expressed by the equilibrium terms as follows.

$$F_{j+\frac{1}{2}}^{E} = \begin{pmatrix} \bar{\rho}\bar{U} \\ \bar{\rho}\bar{U}^2 + \bar{P} \\ \bar{\rho}\bar{E}\bar{U} + \bar{P}\bar{U} \end{pmatrix}.$$

In fact, the numerical flux of the BGK scheme can be thought as some linear combination between the non-equilibrium and equilibrium terms:

$$F_{j+\frac{1}{2}} = \eta F_{j+\frac{1}{2}}^{K} + (1-\eta)F_{j+\frac{1}{2}}^{E}, \qquad (2.6)$$

where $\eta \in [0,1]$. We point out here that in the above flux expression of both KFVS and BGK schemes, $\lambda = \rho/(2P)$, which does not depend on the form of EOS directly. This inspires us to extend the schemes to more general equations of state.

It seems that this kinetic scheme of splitting type can be directly extended to more general EOS. In fact, such (quasi-conservative) splitting kinetic schemes including KFVS, BGK and MKFVS work well for single fluids, but may fail for multi-component flows when the variation of the parameters between EOS of each fluid is big. Fig. 2.1 shows the results calculated by the quasi-conservative MKFVS scheme for a gas-liquid shock tube problem tested in Section 4 (Example 4.5) where the parameters in different EOS are very big. We observe that in a few time step, the pressure become negative and the computation breaks down. The same phenomenon is also observed for the KFVS and BGK schemes. One of the reasons for this failure is maybe that the numerical diffusion is not properly designed. Thus, our idea to remedy the splitting kinetic scheme is to properly enlarge the scheme diffusion. This will be done in the next section.
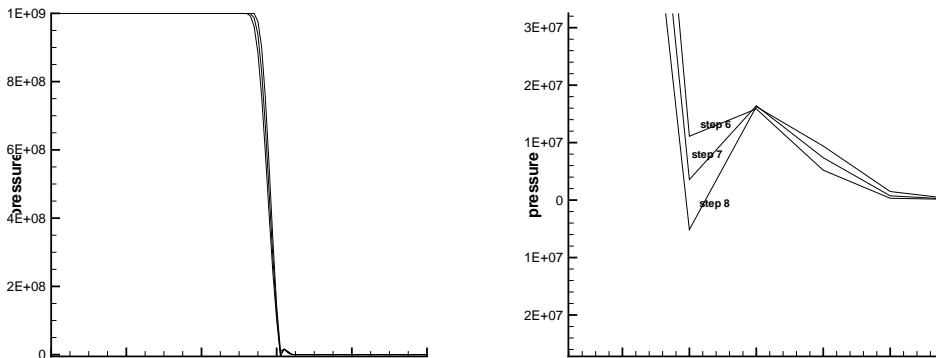
Fig. 2.1. A extreme multi-component fluid problem with stiffened gas EOS: Pressure evaluation in a few steps using the quasi-conservative kinetic scheme

3. A Non-oscillatory Kinetic Scheme for General EOS

In this section, we will discuss how to extend the KFVS scheme to the numerical solution of problems with more general EOS.

3.1. A consistent condition for the KFVS scheme

Adapting the analysis in [20], we first use an interface only model to analyze the mechanism inducing spurious oscillations near a contact discontinuity of the traditional GKS scheme (even) for a single fluid. In fact, if the initial data are chosen as the interface only model, it is equivalent to let U =const and P =const in the Euler equations. Thus,

$$U_x = 0, \quad P_x = 0.$$

Hence, the mass equation reduces to

$$0 = \rho_t + (\rho U)_x = \rho_t + U(\rho)_x. \tag{3.1}$$

Similarly, the momentum equation becomes

$$0 = (\rho U)_t + (\rho U^2 + P)_x = \rho U_t + U\rho_t + U(\rho U)_x + \rho U U_x = \rho U_t,$$

hence, $U_t = 0$.

In the same way, the energy equation becomes

$$0 = (\rho E)_t + (\rho E U + P U)_x = (\rho e)_t + U(\rho e)_x.$$

In the case of the interface only model, the mass equation reduces to a linear equation with constant coefficient U, and we assume $U \equiv 1$ without lose of generality. In this case, the KFVS scheme for the mass equation can be written as

$$\frac{\rho_j^{n+1} - \rho_j^n}{\Delta t} + \frac{(\rho U)_{j+\frac{1}{2}} - (\rho U)_{j-\frac{1}{2}}}{\Delta x} = 0,$$

where

$$(\rho U)_{j+\frac{1}{2}} = \rho_j \langle u^1 \rangle_{j,+} + \rho_{j+1} \langle u^1 \rangle_{j+1,-},$$

$$\langle u^1 \rangle_{j,+} = U_j \langle u^0 \rangle_{j,+} + \frac{e^{-\lambda_{j,+} U_j^2}}{2\sqrt{\pi \lambda_{j,+}}}, \qquad \langle u^0 \rangle_{j,+} = \frac{1}{2}\mathrm{erfc}(-\sqrt{\lambda_{j,+}} U_j),$$

$$\langle u^1 \rangle_{j+1,-} = U_{j+1} \langle u^0 \rangle_{j+1,-} - \frac{e^{-\lambda_{j+1,-} U_{j+1}^2}}{2\sqrt{\pi \lambda_{j+1,-}}}, \qquad \langle u^0 \rangle_{j+1,-} = \frac{1}{2}\mathrm{erfc}(\sqrt{\lambda_{j+1,-}} U_j).$$

After a simple calculation, the above equation becomes

$$\rho_j^{n+1} = \rho_j - \sigma[(\rho_j \langle u^1 \rangle_{j,+} + \rho_{j+1} \langle u^1 \rangle_{j+1,-}) - (\rho_{j-1} \langle u^1 \rangle_{j-1,+} + \rho_j \langle u^1 \rangle_{j,-})]$$

$$= A\rho_j + B\rho_{j+1} + C\rho_{j-1}, \tag{3.2a}$$

$$A = 1 - \sigma[\langle u^1 \rangle_{j,+} - \langle u^1 \rangle_{j,-}], \quad B = -\sigma \langle u^1 \rangle_{j+1,-}, \quad C = \sigma \langle u^1 \rangle_{j-1,+}. \tag{3.2b}$$

According to the basic theory of conservative schemes, the sufficient and necessary condition for the difference equations to be consistent with the corresponding differential equations reads as

$$A + B + C = 1. \tag{3.3}$$

However, for a traditional KFVS scheme, one has $\lambda_{j,+} = \rho_j/(2P_j)$ and $\lambda_{j+1,-} = \rho_{j+1}/(2P_j+1)$, consequently,

$$\lambda_{j,+} \neq \lambda_{j+1,-},$$

which, by recalling (3.2a), shows that the consistent condition (3.3) is not satisfied. The same conclusion also remains true for traditional BGK schemes. So, the traditional KFVS and BGK do not satisfy the consistent condition (3.3). This is exactly the reason why a traditional KFVS may produce spurious oscillations in the vicinity of contact discontinuities. And this also explains why the MKFVS scheme constructed in [2] can avoid oscillations, since it is consistent with the differential equations.

There are a number of ways to make the consistent condition (3.3) satisfied. One simple remedy was given in [2]. In Subsection 3.4 we will provide a more general choice of λ to make the consistent condition be satisfied. In fact, once the following relation

$$\lambda_{j,+} = \lambda_{j+1,-} =: \lambda_{j+\frac{1}{2}} \tag{3.4}$$

holds, the consistent condition (3.3) automatically remains true. Therefore, we will use λ as an independent variable to investigate kinetic schemes. Before doing this, we discuss the truncation error of the kinetic schemes.

3.2. Truncation error of kinetic schemes

In this subsection, we discuss the truncation error of the KFVS-type scheme only. For simplicity, let $U \equiv 1$ and denote

$$\langle u^0 \rangle_{j,+} = \frac{1}{2}\mathrm{erfc}(-\sqrt{\lambda_{j+\frac{1}{2}}}U_j) = \frac{1}{2}\mathrm{erfc}(-\sqrt{\lambda_{j+\frac{1}{2}}}) =: \alpha_{j+\frac{1}{2}},$$

$$\frac{e^{-\lambda_{j+\frac{1}{2}}U_j^2}}{2\sqrt{\pi\lambda_{j+\frac{1}{2}}}} = \frac{e^{-\lambda_{j+\frac{1}{2}}}}{2\sqrt{\pi\lambda_{j+\frac{1}{2}}}} =: \beta_{j+\frac{1}{2}},$$

$$\langle u^1 \rangle_{j,+} = U_j\langle u^0 \rangle_{j,+} + \frac{e^{-\lambda_{j+\frac{1}{2}}U_j^2}}{2\sqrt{\pi\lambda_{j+\frac{1}{2}}}} = \alpha_{j+\frac{1}{2}} + \beta_{j+\frac{1}{2}} =: \theta.$$

Then, it is easy to see that θ is monotone-decreasing in $\lambda_{j+\frac{1}{2}} \in (0, +\infty)$ with infinimum 1.

As $U_j = \langle u^1 \rangle_{j,+} + \langle u^1 \rangle_{j,-}$, we have

$$\langle u^1 \rangle_{j,-} = U_j - \langle u^1 \rangle_{j,+} = 1 - \theta.$$

In order to satisfy the consistent condition (3.3), one should require

$$\langle u^1 \rangle_{j,+} + \langle u^1 \rangle_{j+1,-} = U_{j+\frac{1}{2}} = 1,$$

whence,

$$\langle u^1 \rangle_{j+1,-} = 1 - \langle u^1 \rangle_{j,+} = 1 - \theta.$$

Similarly, to make (3.3) hold, we should have

$$\langle u^1 \rangle_{j-1,+} + \langle u^1 \rangle_{j,-} = U_{j-\frac{1}{2}} = 1,$$

which implies

$$\langle u^1 \rangle_{j-1,+} = 1 - \langle u^1 \rangle_{j,-} = 1 - (1 - \theta) = \theta.$$

Consequently,

$$(\rho U)_{j+\frac{1}{2}} = \rho_j\langle u^1 \rangle_{j,+} + \rho_{j+1}\langle u^1 \rangle_{j+1,-} = \rho_j\theta + \rho_{j+1}(1 - \theta),$$

$$(\rho U)_{j-\frac{1}{2}} = \rho_{j-1}\langle u^1 \rangle_{j-1,+} + \rho_j\langle u^1 \rangle_{j,-} = \rho_{j-1}\theta + \rho_j(1 - \theta).$$

Thus, the KFVS-type kinetic scheme for the mass equation becomes

$$\frac{\rho_j^{n+1} - \rho_j^n}{\Delta t} + \frac{(\rho U)_{j+\frac{1}{2}} - (\rho U)_{j-\frac{1}{2}}}{\Delta x}$$

$$= \frac{\rho_j^{n+1} - \rho_j^n}{\Delta t} + \frac{(\rho_j \theta + \rho_{j+1}(1-\theta)) - (\rho_{j-1}\theta + \rho_j(1-\theta))}{\Delta x}$$

$$= \frac{\rho_j^{n+1} - \rho_j^n}{\Delta t} + \frac{\rho_j(2\theta - 1) + \rho_{j+1}(1-\theta) - \rho_{j-1}\theta}{\Delta x}.$$

The above formulation can be also written as

$$\rho_j^{n+1} = \rho_j - \sigma(\rho_j(2\theta - 1) + \rho_{j+1}(1-\theta) - \rho_{j-1}\theta)$$

$$= \rho_j(1 - \sigma(2\theta - 1)) - \rho_{j+1}\sigma(1-\theta) + \rho_{j-1}\sigma\theta. \tag{3.5}$$

Since $\theta \geqslant 1$, if the following inequality

$$2\theta - 1 \leqslant \max_j\{|U_j| + c_j\} = 1 + \max_j\{c_j\}$$

holds, then all the three coefficients: $(1 - \sigma(2\theta - 1))$, $-\sigma(1-\theta)$ and $\sigma\theta$ in (3.5) are nonnegative. Therefore, the scheme (3.5) is monotone-preserving, and the truncation error will reach its minimum when the scheme reduces to a up-wind scheme (Godunov's theorem, 1959).

Using the Taylor expansion, we find that

$$\rho_j^{n+1} = \rho_j^n + \Delta t\frac{\partial \rho}{\partial t} + \frac{\Delta t^2}{2}\frac{\partial^2 \rho}{\partial t^2} + \cdots,$$

$$\rho_{j\pm1} = \rho_j \pm \Delta x\frac{\partial \rho}{\partial x} + \frac{\Delta x^2}{2}\frac{\partial^2 \rho}{\partial x^2} + \cdots.$$

Hence, the truncation error reads as

$$\frac{\rho_j^{n+1} - \rho_j^n}{\Delta t} + \frac{(\rho U)_{j+\frac{1}{2}} - (\rho U)_{j-\frac{1}{2}}}{\Delta x}$$

$$= \frac{\rho_j^{n+1} - \rho_j^n}{\Delta t} + \frac{(\rho_j \theta + \rho_{j+1}(1-\theta)) - (\rho_{j-1}\theta + \rho_j(1-\theta))}{\Delta x}$$

$$= \frac{\rho_j^{n+1} - \rho_j^n}{\Delta t} + \frac{\rho_j(2\theta - 1) + \rho_{j+1}(1-\theta) - \rho_{j-1}\theta}{\Delta x}$$

$$= \frac{\partial \rho}{\partial t} + \frac{\partial^2 \rho}{\partial t^2}\frac{\Delta t}{2} + \frac{\partial \rho}{\partial x} + \frac{\partial^2 \rho}{\partial x^2}\frac{\Delta x}{2}(1 - 2\theta) + \cdots$$

$$= \frac{\partial^2 \rho}{\partial t^2}\frac{\Delta t}{2} + \frac{\partial^2 \rho}{\partial x^2}\frac{\Delta x}{2}(1 - 2\theta) + \cdots = \frac{\Delta x}{2}\frac{\partial^2 \rho}{\partial x^2}(\sigma + 1 - 2\theta) + \cdots.$$

So, the range of $\sigma + 1 - 2\theta$ will effect the range of the truncation error. Since the coefficient in the last line of the above identity is always negative, and θ is monotone-decreasing in $\lambda_{j+\frac{1}{2}} \in (0, +\infty)$ and the infimum of θ in λ is 1. Obviously, $\theta = 1$ when $\lambda \to \infty$. In this case, the scheme reduces to a up-wind scheme, the truncation error reach its minimum. In contrast, when λ is getting small, the truncation error becomes large, the dissipation of the scheme thus will be large.

3.3. Positivity analysis for the kinetic scheme

In this section we analyze the positivity of the KFVS-type scheme. As mentioned above, the KFVS-type scheme can be written as

$$\rho_j^{n+1} = A\rho_j + B\rho_{j+1} + C\rho_{j-1},$$

where

$$A = 1 - \sigma(\langle u^1 \rangle_{j,+} - \langle u^1 \rangle_{j,-}),$$
$$B = -\sigma \langle u^1 \rangle_{j+1,-} \geq 0,$$
$$C = \sigma \langle u^1 \rangle_{j-1,+} \geq 0.$$

Therefore, if $A \geq 0$, then the density is positive. In order to guarantee $A \geq 0$, we only need, by virtue of the stability condition of the scheme, that

$$\langle u^1 \rangle_{j,+} - \langle u^1 \rangle_{j,-} \leq \max\{|U_j| + c_j\},$$

where c is the speed of sound. Since

$$\langle u^1 \rangle_{j,+} - \langle u^1 \rangle_{j,-} = U_j(\langle u^0 \rangle_{j,+} - \langle u^0 \rangle_{j,-}) + \frac{e^{-\lambda_{j,+} U_j^2}}{2\sqrt{\pi \lambda_{j,+}}} + \frac{e^{-\lambda_{j,-} U_j^2}}{2\sqrt{\pi \lambda_{j,-}}}$$

$$\leq |U_j| + \frac{1}{2\sqrt{\pi \lambda_{j,+}}} + \frac{1}{2\sqrt{\pi \lambda_{j,-}}},$$

we have

$$\frac{1}{\sqrt{\pi \lambda_{j,\pm}}} \leq \max\{c_j, c_{j+1}\}.$$

Let $\lambda_{j,+} = \lambda_{j+1,-} =: \lambda_{j+\frac{1}{2}}$, then

$$\lambda_{j+\frac{1}{2}} \geq \min\left\{\frac{1}{c_j^2}, \frac{1}{c_{j+1}^2}\right\}/\pi. \tag{3.6}$$

Hence, if the condition (3.6) is satisfied, then the positivity of the density is preserved. According to the analysis in the previous section, the dissipation of the scheme will get large if λ becomes small. This enhances the ability of the scheme to deal with strong shock waves.

3.4. A non-oscillatory kinetic scheme

In this section, based on the previous analysis, we will propose a new non-oscillatory kinetic scheme by choosing λ appropriately. We have carried out a number of numerical tests and find that it is suitable to choose

$$\lambda_{j,+} = \lambda_{j+1,-} =: \lambda_{j+\frac{1}{2}} = \min\left\{\frac{1}{c_j^2}, \frac{1}{c_{j+1}^2}\right\}.$$

Then, the new scheme reads as

$$\vec{W}_j^{n+1} = \vec{W}_j^n - \lambda[F_{j+\frac{1}{2}} - F_{j-\frac{1}{2}}],$$

where the numerical flux is composed of two parts

$$F_{j+\frac{1}{2}} = \eta F_{j+\frac{1}{2}}^K + (1 - \eta)F_{j+\frac{1}{2}}^E.$$

The non-equilibrium part is

$$F_{j+\frac{1}{2}}^K = F_j^+ + F_{j+1}^-,$$

where

$$F_j^{\pm} = \langle u^1 \rangle_{j,\pm}^{new} \begin{bmatrix} \rho \\ \rho U \\ \rho E \end{bmatrix}_j + \begin{bmatrix} 0 \\ P_j \langle u^0 \rangle_{j,\pm}^{new} \\ \frac{1}{2} P_j \langle u^1 \rangle_{j,\pm}^{new} + \frac{1}{2} P_j U_j \langle u^0 \rangle_{j,\pm}^{new} \end{bmatrix},$$

and

$$\langle u^n \rangle_{j,\pm}^{new} = \langle u^n \rangle_{j,\pm}^*,$$

$$\langle u^0 \rangle_{j,\pm}^* = \frac{1}{2}\text{erfc}(\mp\sqrt{\lambda_{j,\pm}^*}U_j),$$

$$\langle u^1 \rangle_{j,\pm} = U_j \langle u^0 \rangle_{j,\pm} \pm \frac{1}{2}\frac{e^{-\lambda_{j,\pm}^* U_j^2}}{\sqrt{\pi}\lambda_{j,\pm}^*},$$

$$\langle u^0 \rangle_{j,\pm}^* = \frac{1}{2}\text{erfc}(\mp\sqrt{\lambda_{j,\pm}^*}U_j),$$

$$\langle u^1 \rangle_{j,\pm}^* = U_j \langle u^0 \rangle_{j,\pm}^* \pm \frac{1}{2}\frac{e^{-\lambda_{j,\pm}^* U_j^2}}{\sqrt{\pi}\lambda_{j,\pm}^*},$$

$$\lambda_{j,+}^* = \lambda_{j+1,-}^* =: \lambda_{j+\frac{1}{2}} = \min\left\{\frac{1}{c_j^2}, \frac{1}{c_{j+1}^2}\right\}.$$

In order to avoid oscillations of the pressure and velocity near a contact discontinuity, the equilibrium part should also satisfy the consistent condition. Slightly different from Xu's BGK scheme [36], we first calculate the following terms

$$\begin{pmatrix} \bar{\rho} \\ \bar{U} \\ \bar{P} \end{pmatrix}_{j+\frac{1}{2}} = \begin{pmatrix} \rho_j \langle u^0 \rangle_{j,+}^* + \rho_{j+1} \langle u^0 \rangle_{j+1,-}^* \\ \langle u^1 \rangle_{j,+}^* + \langle u^1 \rangle_{j+1,-}^* \\ P_j \langle u^0 \rangle_{j,+}^* + P_{j+1} \langle u^0 \rangle_{j+1,-}^* \end{pmatrix}.$$

Consequently, we take

$$F_{j+\frac{1}{2}}^E = \begin{pmatrix} \bar{\rho} \\ \bar{\rho}\bar{U} \\ \bar{\rho}\bar{E} \end{pmatrix}_{j+\frac{1}{2}},$$

where $\bar{E}$ is determined by EOS.

Thus, we have constructed a new kinetic scheme and we call it the non-oscillation kinetic (NOK) scheme. For this NOK scheme, once the speed of sound is known, the numerical flux can be obtained; and the particle distribution function in equilibrium state is actually not needed in the construction of the numerical flux. Therefore, it can be used in the numerical simulation of fluid problems with general EOS.

3.5. A quasi-conservative NOK scheme for the extended Euler equations with EOS for a stiffened gas

In this section we will give a quasi-conservative NOK scheme for the multi-component extended Euler equations with EOS for a stiffened gas by utilizing the idea from [30].

The Mie-Grüneisen EOS is used to describe a wide range of real materials including gases, liquids and solids. The uniform Mie-Grüneisen EOS can be written as

$$P(\rho, e) = \text{P}_{\text{ref}}(\rho) + \Gamma(\rho)\rho[e - e_{\text{ref}}(\rho)],$$

where $\Gamma(\rho)$ is the Mie-Grüneisen coefficient, $\text{P}_{\text{ref}}(\rho)$ and $e_{\text{ref}}(\rho)$ are the reference pressure and internal energy.

When the material density is not far away from the reference density, one usually uses the following simplified EOS, called the equation of state for a stiffened gas, to replace the more complex Mie-Grüneisen EOS,

$$P = (\gamma - 1)\rho e - \gamma P_\infty, \tag{3.7}$$

where when $P_\infty = 0$, the EOS (3.7) reduces to that for an ideal gas. This EOS is a suitable approximation for gases, liquid and solid under high pressure. The parameter in (3.7) can be adjusted to agree with experiment data, see [29] for some examples. And since it is easy to construct the exact Riemann solver, the EOS for a stiffened gas is often used to validate the efficiency and correctness of a numerical scheme. In this section, we will extend the NOK scheme to the multi-component extended Euler equations with EOS for a stiffened gas.

Following the process in [30], the model of the multi-component extended Euler equations with EOS for a stiffened gas consists of two parts: the original Euler equations and the species equations. There are two models for the species equations, i.e.,

$$\begin{cases} \dfrac{\partial}{\partial t}\left(\dfrac{1}{\gamma - 1}\right) + U\dfrac{\partial}{\partial x}\left(\dfrac{1}{\gamma - 1}\right) = 0, \\[3mm] \dfrac{\partial}{\partial t}\left(\dfrac{\gamma P_\infty}{\gamma - 1}\right) + U\dfrac{\partial}{\partial x}\left(\dfrac{\gamma P_\infty}{\gamma - 1}\right) = 0, \end{cases}$$

or

$$\frac{\partial Y}{\partial t} + U\frac{\partial Y}{\partial x} = 0,$$

where Y is the volume-fraction or mass fraction of some component of the fluid. The above two models are equivalent, and here we choose the mass fraction model.

The basic idea to construct a quasi-conservative scheme is similar to that in [2]. We first discretize the original Euler equations using the NOK scheme proposed in the previous section. Then, the species equation is rewritten as

$$0 = \frac{\partial Y}{\partial t} + U\frac{\partial Y}{\partial x} = \frac{\partial Y}{\partial t} + \frac{\partial (UY)}{\partial x} - Y\frac{\partial U}{\partial x},$$

and discretized as follows.

$$\begin{aligned} Y_j^{n+1} = Y_j^n - \sigma\Big\{ &\left[(Y_j\langle u^1\rangle_{j,+} + Y_{j+1}\langle u^1\rangle_{j+1,-}) - (Y_{j-1}\langle u^1\rangle_{j-1,+} + Y_j\langle u^1\rangle_{j,-})\right] \\ &+ Y_j\left[(\langle u^1\rangle_{j,+} + \langle u^1\rangle_{j+1,-}) - (\langle u^1\rangle_{j-1,+} + \langle u^1\rangle_{j,-})\right]\Big\}, \end{aligned}$$

and γ and P_∞ are determined by

$$\frac{1}{\gamma - 1} = \frac{Y}{\gamma^{(1)} - 1} + \frac{1 - Y}{\gamma^{(2)} - 1},$$

$$\frac{\gamma P_\infty}{\gamma - 1} = \frac{\gamma^{(1)} P_\infty^{(1)}}{\gamma^{(1)} - 1}Y + \frac{\gamma^{(2)} P_\infty^{(2)}}{\gamma^{(2)} - 1}(1 - Y),$$

where (i) denotes the i-th component.

4. Numerical Tests

In this section, we will present a number of numerical tests of multi-component problems to demonstrate the accuracy and robustness of our quasi-conservative NOK scheme. We begin with one-dimensional problems.

4.1. 1D tests

Example 4.1. Interface only problem. For this problem, the initial data are given by

$$(\rho, U, P, \gamma, P_\infty) = \begin{cases} (1, 1, 1, 1.4, 1), & x < 0.5, \\ (0.125, 1, 1, 1.9, 0), & x > 0.5. \end{cases}$$

We take $\eta = 1.0$ and $\eta = 0.5$ in the NOK scheme, respectively. When $\eta = 1.0$, the equilibrium term vanishes, and in this case we denote the scheme by NOK-I; while when $\eta = 0.5$, the equilibrium term goes into effect, and in this case we denote the scheme by NOK-II. The computation is carried out on a uniform mesh with 100 cells. The CFL number is chosen to be 0.9 for the first-order scheme and 0.7 for the second-order scheme, respective. In Fig. 4.1 and 4.2 the numerical results at time $t = 0.1$ are shown. Obviously, there is no spurious oscillation across the material interface in the velocity and pressure, and the second-order scheme resolves better than the first-order scheme. To compare the accuracy of the NOK-I and NOK-II schemes, we give the close-up of the density near the material interface in Fig. 4.3, from which we observe that although the difference in accuracy between two schemes is small, the NOK-II scheme, which takes into account the equilibrium state, shows less dissipative than the NOK-I scheme which does not take into account the equilibrium state. Furthermore, if η is chosen properly, the NOK-II scheme may behave better in the regions of smooth solution or moderate shock waves than the NOK-I scheme. However, it reduces to NOK-I in the regions of strong shock waves in order to avoid unphysical oscillations behind a shock wave.
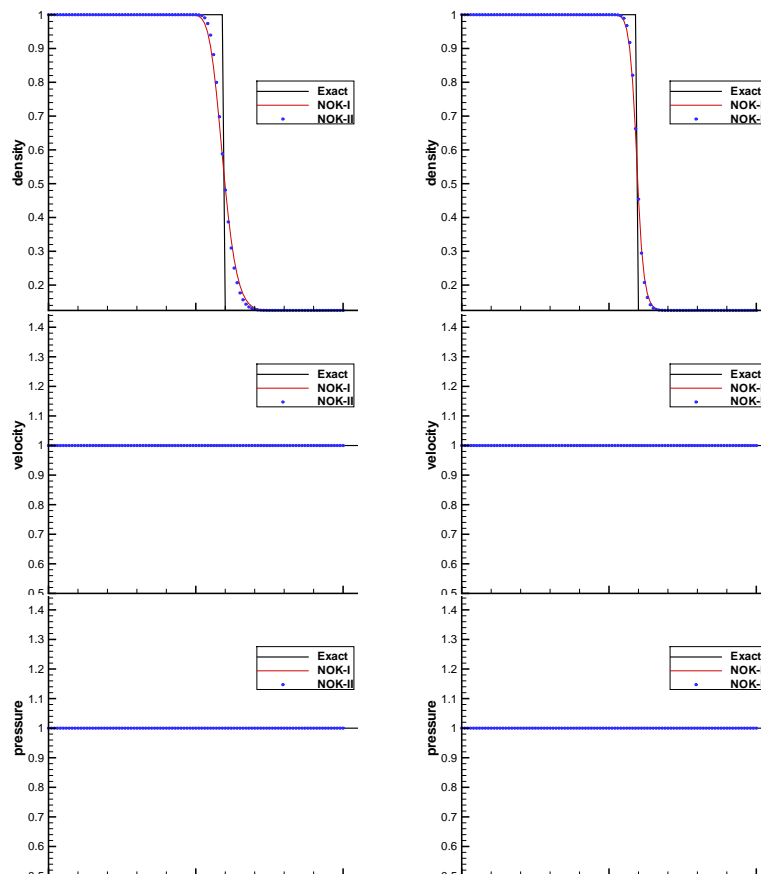
Fig. 4.1. Example 4.1. Left resp. Right: Computed density, velocity and pressure by the NOK-I resp. NOK-II schemes. Thick solid line: Exact solution. Thin solid line: Results obtained by using the NOK-I scheme. Points: Results computed by using the NOK-II scheme.
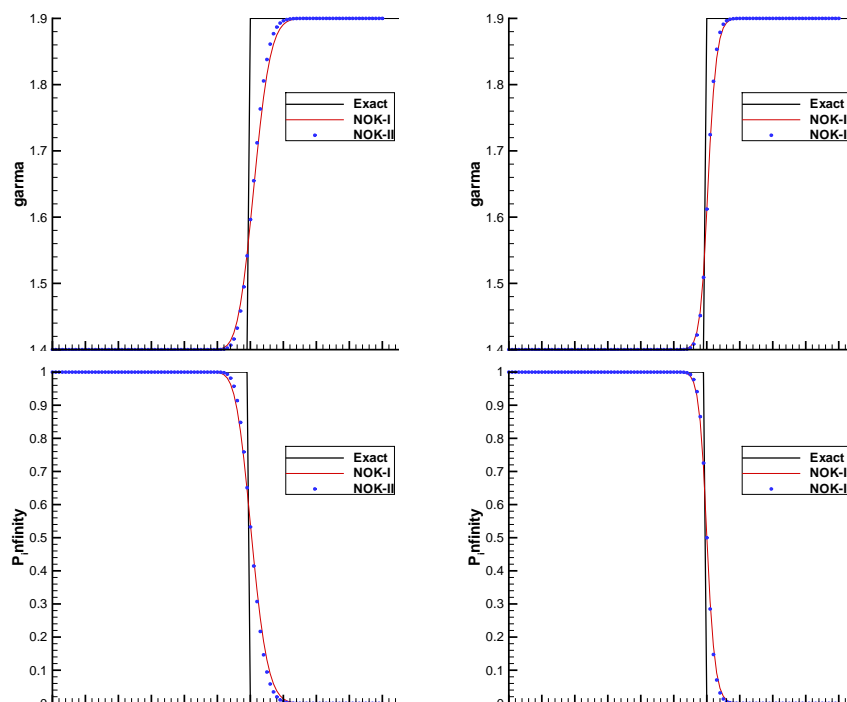
Fig. 4.2. Example 4.1. (continue) Left: Computed γ and P_∞ by the NOK-I scheme. Right: Computed γ and P_∞ by the NOK-II scheme. Thick solid line: Exact solution. Thin solid line: Results computed by using the NOK-I scheme. Points: Results obtained by using the NOK-II scheme.
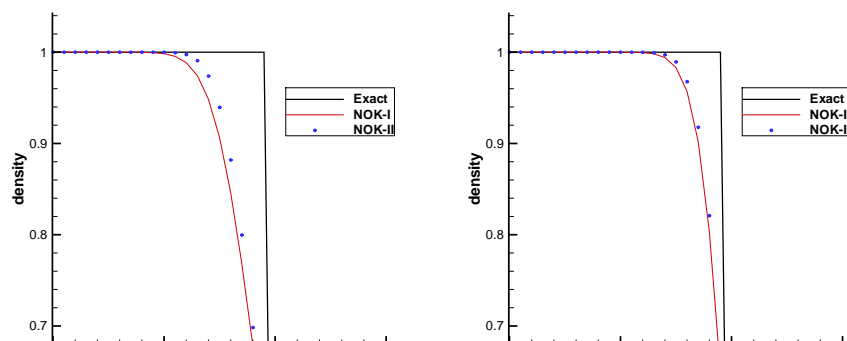
Fig. 4.3. Example 4.1. Close-up of the density near the material interface. Left: Computed results by using the first-order scheme. Right: Results obtained by the second-order scheme.

Example 4.2. Gas-liquid shock tube test I: moderate shock waves

This is a difficult test example due to the large difference of the physical characters between gases and liquids, and had been considered as a underwater explosive problem with two-dimensional spherically symmetric geometry [4]. For this problem, the initial data are

$$(\rho, U, P, \gamma, P_\infty) = \begin{cases} (1.241, 0, 2.753, 1.4, 0), & x < 0.5, \\ (0.991, 0, 3.059e - 4, 5.5, 1.505), & x > 0.5. \end{cases} \quad (4.1)$$

We set $\eta = 1.0$ and $\eta = 0.7$ in the NOK scheme, and denote the NOK scheme with $\eta = 1.0$ by NOK-I and with $\eta = 0.7$ by NOK-II. We should point out here that η should not be set too
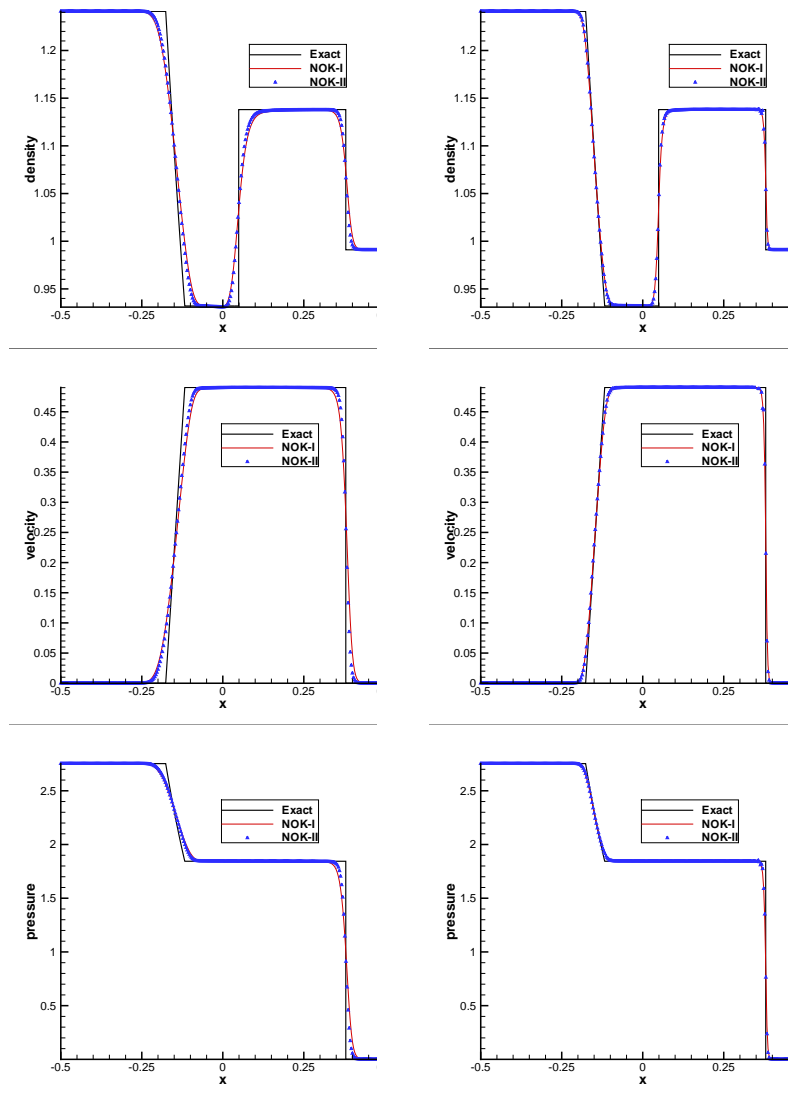
Fig. 4.4. Example 4.2. Numerical results of the density, velocity and pressure at $t = 0.1$. Left: 1st-order scheme; Right: 2nd-order scheme. Thick solid line: Exact solution; Thin solid line: NOK-I scheme; Triangles: NOK-II scheme.

small. Otherwise, oscillations behind the shock wave could appear. A more detailed analysis on the choice of η is a topic for the future study.

We carry out the computation with 600 cells for the first-order scheme and 300 cells for the second-order one, and take the CFL number to be 0.7 for the first-order scheme and 0.5 for the second-order one. The numerical results are presented in Fig. 4.4. It is clear to see that the numerical solution approaches the exact one. Fig. 4.5 shows the close-up of the density in the vicinity of the material interface in order to give a comparison between the NOK-I and NOK-II schemes in detail. Although the difference in accuracy between two schemes is small, the NOK-II is obviously less dissipative than the NOK-I.
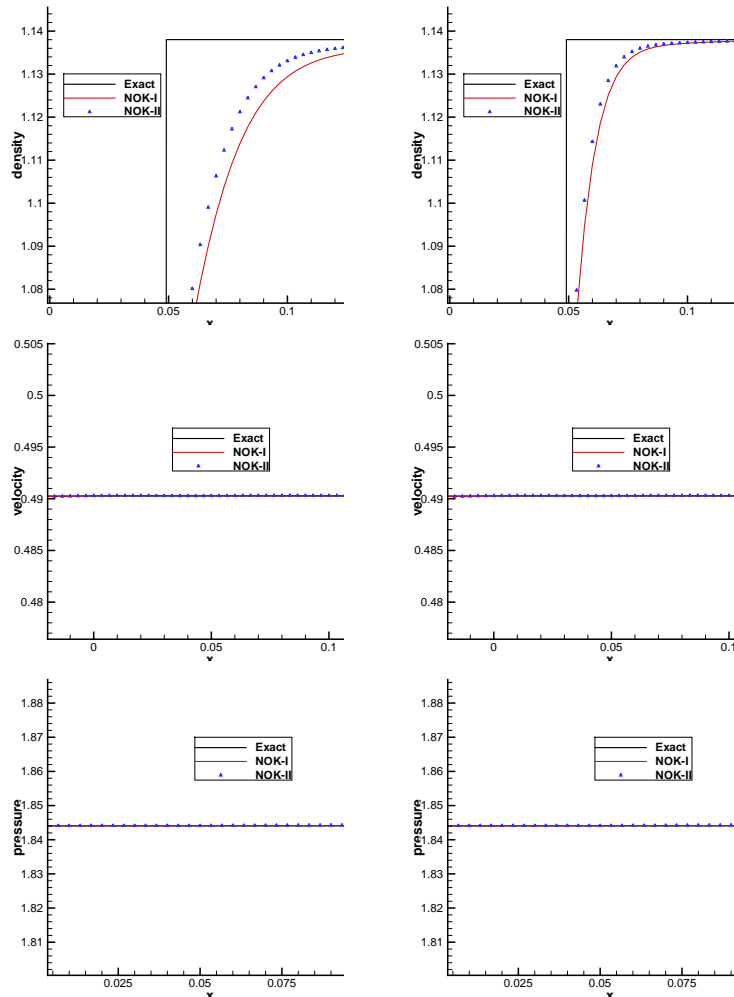
Fig. 4.5. Example 4.2. Close-up of the computed density, velocity and pressure near the contact discontinuity. Left: 1st-order scheme; Right: 2nd-order scheme. Thick solid line: Exact solution; Thin solid line: NOK-I scheme; Triangles: NOK-II scheme.

Example 4.3. Gas-liquid shock tube test II: strong shock waves.

We continue to test our scheme for a gas-liquid shock tube problem with a strong shock wave, where the density ratio is very large. The numerical simulation of such problems is challenging, and the usual quasi-conservative kinetic schemes such as the KFVS, BGK and MKFVS schemes can result in negative pressure, cf. Fig. 1.

For this example, the initial setting is a water–air shock tube given by

$$(\rho, U, P, \gamma, P_\infty) = \begin{cases} (1000, 0, 1.0e+9, 4.4, 6.0e+8), & x < 0.5, \\ (1, 0, 1.0e+5, 1.4, 0.0), & x > 0.5. \end{cases}$$

The initial conditions will soon generate a nearly centered wave system which consists of a rarefaction wave, a contact discontinuity and a strong shock wave. Since the equilibrium state will vanish in the regions of the strong shock wave, we carry out simulations only for $\eta = 1.0$ to enhance dissipation. In Fig. 4.6, the numerical results of the first- and second-order NOK schemes using 10000 cells are given. From Fig. 4.6, we see that the numerical results approach
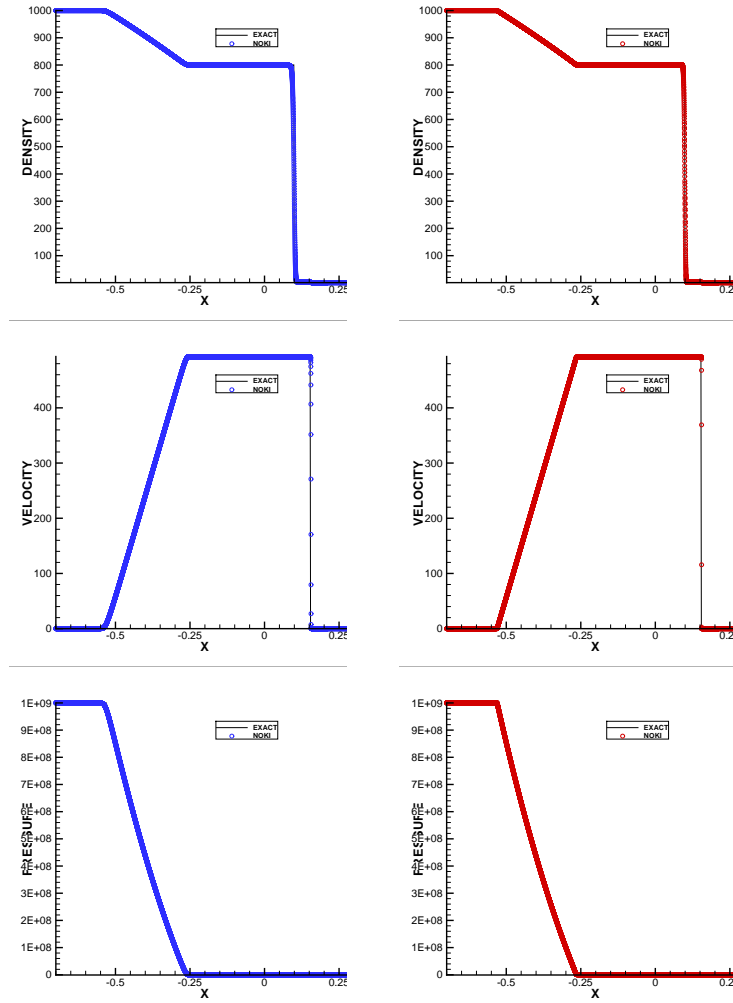
Fig. 4.6. Example 4.3. Numerical results of the density, velocity and pressure at $t = 2.0$e-4. Left: 1st-order NOK scheme; Right: 2nd-order NOK scheme. Solid line: Exact solution; Circles: Computed solution.

the exact solution very well, and the second-order scheme is more accurate than the first-order one in the region of the shock wave. Fig. 8 shows close-up of the material interface, and the second-order scheme also provides higher resolution than the first-order one, and both of them produce no spurious oscillations across the material interface.

Example 4.4. 2D interface only problem.

In this example, we test a 2D extension problem of Example 4.1 with initial data

$$(\rho, U, V, P, \gamma, P_\infty) = \begin{cases} (1, 1, 1, 1, 1.4, 0), & \sqrt{(x - 0.25)^2 + (y - 0.25)^2} < 0.16^2, \\ (0.125, 1, 1, 1, 4, 1), & \sqrt{(x - 0.25)^2 + (y - 0.25)^2} < 0.16^2. \end{cases}$$

In the simulation we take $\eta = 1.0$ and $\eta = 0.5$ in the NOK scheme, and as before, denote the corresponding NOK scheme by NOK-I and NOK-II, respectively. The numerical results of the density and P_∞ obtained by using 100×100 cells are given in Figs. 4.8 and 4.9, from which we
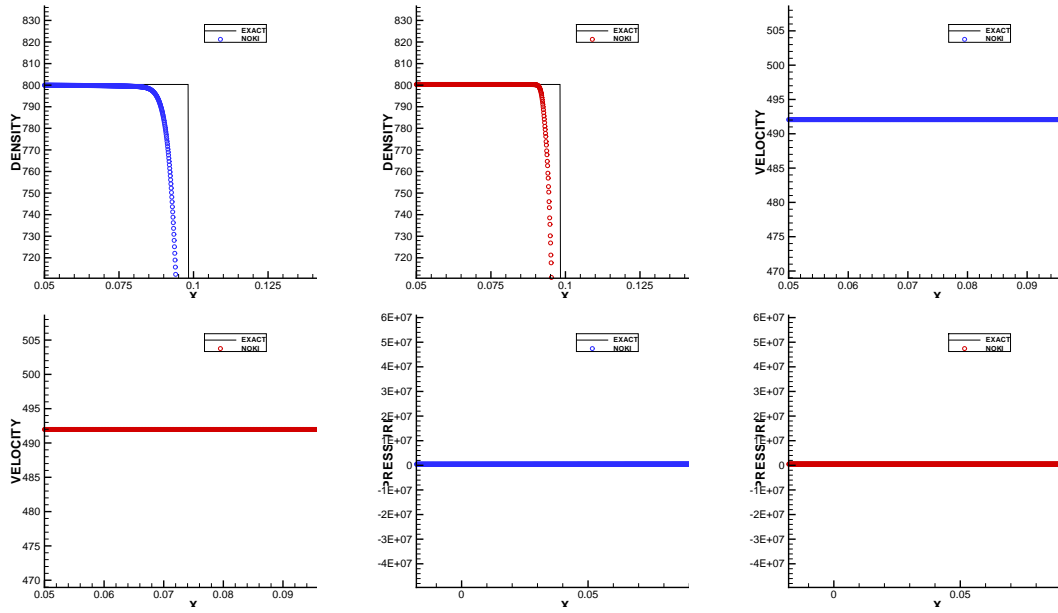
Fig. 4.7. Example 4.3. Close-up of the density, velocity and pressure near the contact discontinuity. Left: 1st-order NOK scheme; Right: 2nd-order NOK scheme. Solid line: Exact solution; Circles: Computed solution.
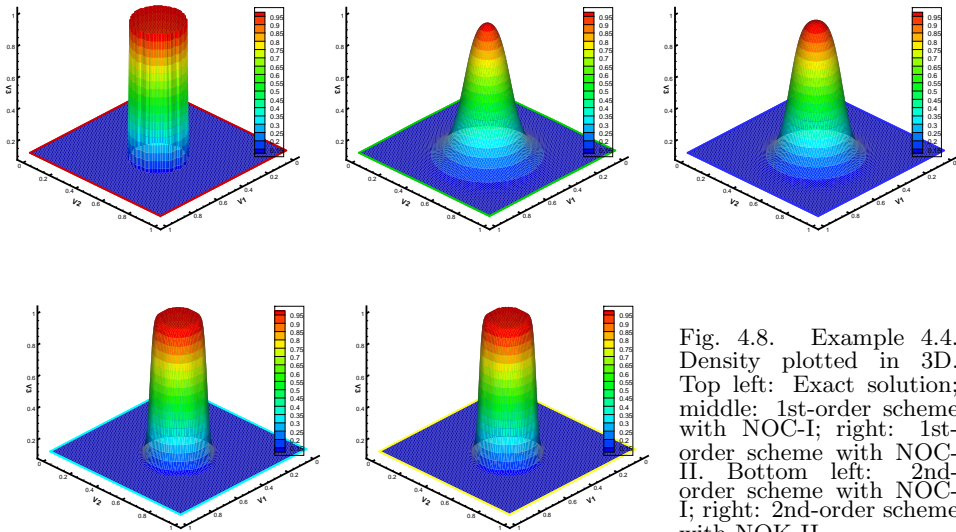
Fig. 4.8. Example 4.4. Density plotted in 3D. Top left: Exact solution; middle: 1st-order scheme with NOC-I; right: 1st-order scheme with NOC-II. Bottom left: 2nd-order scheme with NOC-I; right: 2nd-order scheme with NOK-II.

reach the same conclusion as that for the 1D case, i.e., Example 4.1, namely, the NOK scheme will not produce any spurious oscillations across material interfaces. Our computational results for the pressure and P_∞ provide similar observations.

Example 4.5. Richtmyer-Meshkov instability.

For this problem we take the same computational conditions as in [30] and implement
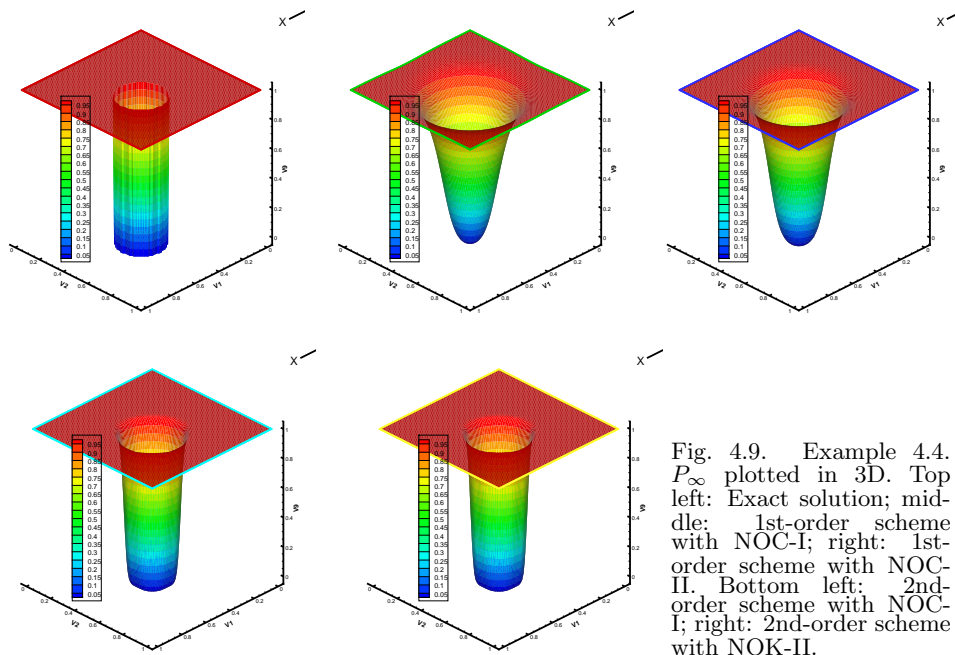
Fig. 4.9. Example 4.4. P_∞ plotted in 3D. Top left: Exact solution; middle: 1st-order scheme with NOC-I; right: 1st-order scheme with NOC-II. Bottom left: 2nd-order scheme with NOC-I; right: 2nd-order scheme with NOK-II.
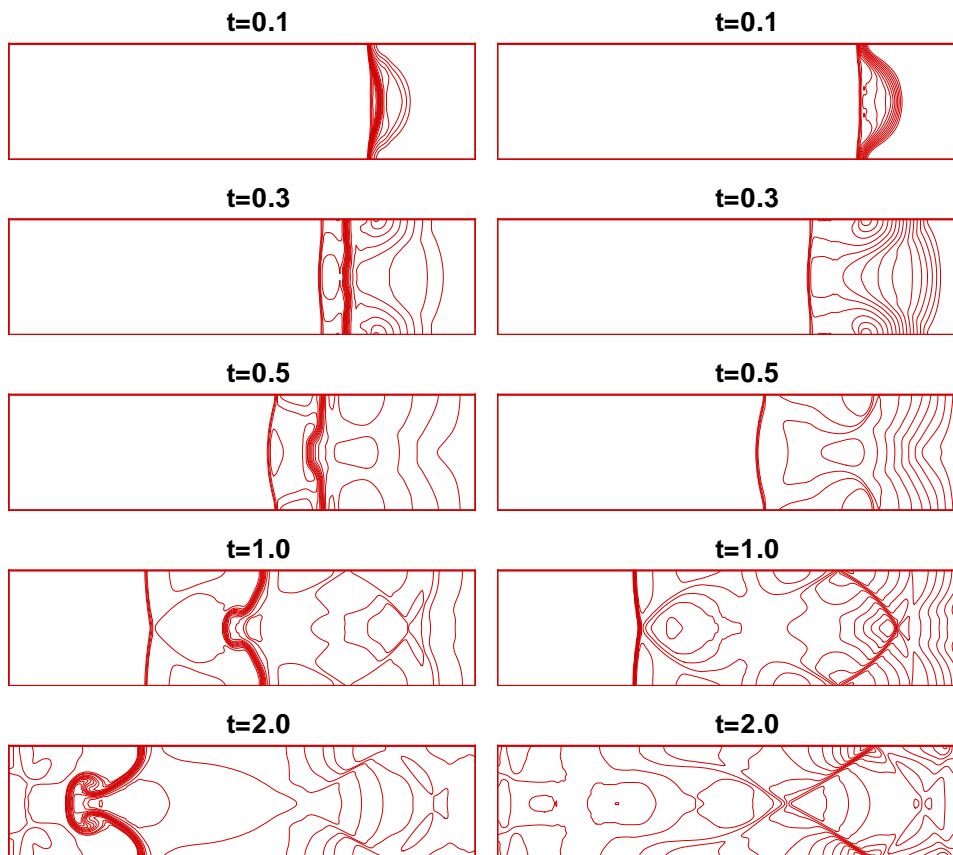
Fig. 4.10. Example 4.5. Results computed by the 2nd-order NOK scheme. Left: Density contours; Right: Pressure contours. From the top down are the numerical results at time $t = 0.1, 0.3, 0.5, 1.0, 2.0$.
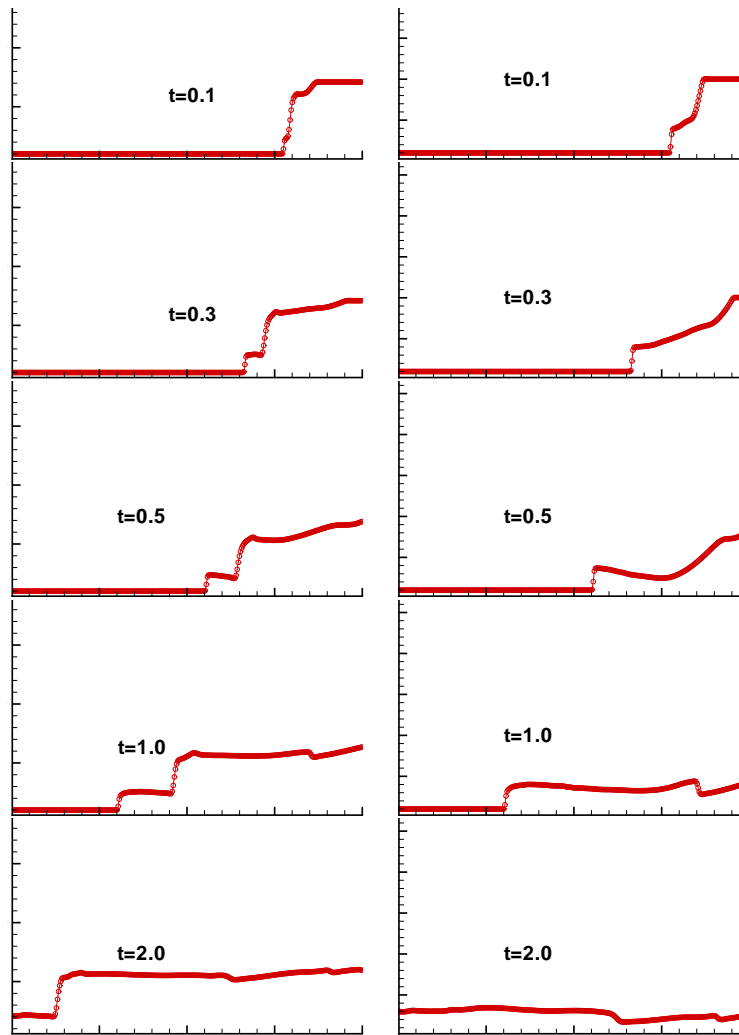
Fig. 4.11. Example 4.5. Cross-sectional plots of the numerical results in Fig. 4.10 along line $y = 0.5$; Left: Density; Right: Pressure.

computation for a single mode perturbation of an air-liquid interface. Initially, the interface is located at

$$x = x_0 + 0.1 \cos(2\pi y) =: f(y),$$

and there is a planar Mach 1.95 shock wave in the air propagating from left toward the interface to trigger the instability. The initial distribution is

$$(\rho, U, V, P, \gamma, P_\infty) = \begin{cases} (1.0, 0, 0, 1.0, 1.4, 0), & x < f(y), \\ (5.0, 0, 0, 1.0, 4.0, 1), & x < 1.325, \\ (7.093, -0.7288, 0, 10.0, 4.0, 1), & \text{else.} \end{cases}$$

The boundary conditions of the top and bottom are periodic, while the left and right are non-reflecting. The wave structure will become very complex when time increases, in particular, after the interface is shifted over 180 degree by a shock wave propagating from the liquid to the air. We use 320×80 cells in the computation. Fig. 4.10 shows the computed density and pressure contours by using the second-order NOK scheme with $\eta = 1.0$ at time $t = 0.1, 0.3, 0.5, 1.0, 2.0$,

while Fig. 4.11 gives the cross-sectional plots of the numerical results in Fig. 4.10 along line $y = 0.5$. Clearly, the results obtained by the second-order NOK scheme here are in good agreement with those in [30], while the interface computed by our scheme is obviously closer to that computed by the tracking method in [30]. This demonstrates the good performance of our NOK scheme.

5. Conclusions

In this article, based a careful analysis of the mechanism inducing oscillations across a contact discontinuity of the traditional kinetic schemes such as the KFVS and BGK schemes (see, e.g., [2]), we have utilized a flux splitting technique to propose a new non-oscillatory kinetic (NOK) scheme for the Euler equations with the equation of state for multi-component stiffened gases. Using the flux splitting, we have constructed the numerical fluxes which do not depend on the concrete form of the equilibrium state. Consequently, our new scheme can deal with stiffened gases, extending the traditional gas kinetic scheme to the stiffened gas case. Furthermore, we have carried out a careful analysis on the consistency condition, truncation error and positivity of the NOK scheme to show that it not only can be used to simulate multi-component flows with the equation of state for a stiffened gas, but also is oscillation-free across a material interface in the pressure and velocity. We have carried out a number of 1D and 2D numerical tests which demonstrate that the new scheme works well in the regions of both smooth solutions and weak/strong shock waves, and is robust and could be suitable for a more general EOS. This is a topic for our future study.

References

[1] R. Abgrall, How to prevent pressure oscillations in multicomponent flow calculation: A quasi conservative approach. *J. Comput. Phys.*, **125** (1996), 150-160.

[2] Y. Chen and S. Jiang, Modified kinetic flux vector splitting schemes for compressible flows. *J. Comput. Phys.*, **228** (2009), 3582-3604.

[3] B.N. Chetverushkin and Kinetic Schemes, Quasi-Gas Dynamic System of Equations, CIMNE Publication, Barcelona, Spain, 2008.

[4] J.P. Cocchi, R. Saurel and J.C. Loraud, Treatment of interface problems with Godunov-type scheme, *Shock Waves*, **5** (1996), 347-357.

[5] G. Cochran and J. Chan, Shock initiation and detonation models in one and two dimensions, *UCID-18024*, LLNL, USA (1979).

[6] S.M. Deshpande, Kinetic theory based new upwind methods for inviscid compressible flows, *AIAA Paper 86-0275*, (1986).

[7] B.M. Dobratz and P.C. Crawford, Explosive handbook of properties of chemical explosives and explosive simulants. *UCRL-52997*, LLNL, USA (1985).

[8] W. Dreyer and S. Qamar, Kinetic flux-vector splitting schemes for the hyperbolic heat conduction, *J. Comput. Phys.*, **198** (2004), 403-423.

[9] T.G. Elizarova, I.A. Graur and J.-C. Lengrand, Two-fluid computational model for a binary gas mixture, *Eur. J. Mech. B-Fluid.*, **20** (2001), 351-369.

[10] T.G. Elizarova, Quasi-Gas Dynamic Equations, Springer Verlag, Berlin, Heidelberg, 2009.

[11] R. Fedkiw, T. Aslam, B. Merriman and S. Osher, A non-oscillatory Eulerian approach to interfaces in multimaterial flows (the Ghost Fluid Method), *J. Comput. Phys.*, **152** (1999), 457-492.

[12] A. Harten, High resolution schemes for hyperbolic conservation laws. *J. Comput. Phys.*, **49** (1983), 357-393.

[13] A. Harten, B. Engquist, S. Osher and R. Chakravarthy, Uniformly high-order accurate essentially non-oscillatory schemes. *J. Comput. Phys.*, **71** (1987), 231-303.

[14] R. Jeanloz, Shock wave equation of state and finite strain theory, *J. Geophys. Res.*, **94** (1989), 5873-5886.

[15] P. Jenny, B. Müller and H. Thomann, Correction of conservative Euler solvers for gas mixtures, *J. Comput. Phys.*, **132** (1997), 91-107.

[16] S. Jiang and G.X. Ni, A γ-model BGK scheme for compressible multifluids, *Int. J. Numer. Meth. Fluids*, **46** (2004), 163-182.

[17] S. Jiang and G.X. Ni, A second-order γ-model BGK scheme for multimaterial compressible flows, *Appl. Numer. Math.*, **57** (2007), 597-608.

[18] C. Jin and K. Xu, An adaptive grid method for two dimensional viscous flows, *J. Comput. Phys.*, **218** (2006), 68-81.

[19] C. Jin and K. Xu, A unified moving grid gas-kinetic method in Eulerian space for viscous flow computation, *J. Comput. Phys.*, **222** (2007), 155-175.

[20] S. Karni, Multi-component flow by a consistent primitive algorithm, *J. Comput. Phys.*, **112** (1994), 31-43.

[21] S. Karni, Hybrid multifluid algorithm, *SIAM J. Sci. Comput.*, **17** (1996), 1019-1039.

[22] Y.S. Lian and K. Xu, A gas-kinetic scheme for multimaterial flows and its application in chemical reactions, *J. Comput. Phys.*, **163** (2000), 349-375.

[23] G.X. Ni, S. Jiang and K. Xu, A DGBGK scheme based on WENO limiters for viscous and inviscid flows, *J. Comput. Phys.*, **227** (2008), 5799-5815.

[24] G.X. Ni, S. Jiang and K. Xu, Remapping-free ALE-type kinetic method for flow computations, *J. Comput. Phys.*, **228** (2009), 3154-3171.

[25] T. Ohwada, On the construction of kinetic scheme. *J. Comput. Phys.*, **177** (2002), 156-175.

[26] T. Ohwada and S. Kobayashi, Management of discontinuous reconstruction in kinetic schemes, *J. Comput. Phys.*, **197** (2004), 116-138.

[27] T. Ohwada and S. Fukata, Simple derivation of high-resolution schemes for compressible flows by kinetic approach, *J. Comput. Phys.*, **211** (2006), 424-447.

[28] T. Ohwada and P. Asinari, Artificial compressibility method revisited: asymptotic numerical method for incompressible Navier-Stokes equations, *J. Comput. Phys.*, **229** (2010), 1698-1723.

[29] R. Saurel and R. Abgrall, A simple method for compressible multifluid flows, *SIAM J. Sci. Comput.*, **21** (1999), 1115-1145.

[30] K.M. Shyue, An efficient shock-capturing algorithm for compressible multicomponent problems, *J. Comput. Phys.*, **142** (1998), 208-242.

[31] K.M. Shyue, A fluid-mixture type algorithm for compressible multicomponent flow with Mie-Gruneisen equation of state, *J. Comput. Phys.*, **171** (2001), 678-707.

[32] K.M. Shyue, A wave-propagation based volume tracking method for compressible multicomponent flow in two space dimensions, *J. Comput. Phys.*, **215** (2006), 219-244.

[33] H.Z. Tang and H.M. Wu, High resolution KFVS finite volume methods for multicomponent flow calculations, *Chinese J. Comput. Phys.*, **117** (2000), 179-186.

[34] H.Z. Tang and H.M. Wu, Kinetic flux vector splitting for radiation hydrodynamical equations, *Comput. Fluids*, **29** (2000), 917-933.

[35] B. van Leer, MUSCL, a new approach to numerical gas dynamics. In *Computing in Plasma Physics and Astrophysics*, Max-Planck-Institut für Plasma Physic, Garchung, Germany, April, 1976.

[36] K. Xu, BGK-based scheme for multicomponent flow calculations, *J. Comput. Phys.*, **134** (1997), 122-133.

[37] K. Xu, Gas kinetic theory based flux splitting method for ideal magnetohydrodynamics, *J. Comput. Phys.*, **153** (1999), 334-352.

[38] K. Xu, A gas-kinetic BGK scheme for the Navier-Stokes equations and its connection with artificial dissipation and Godunov method. *J. Comput. Phys.*, **171** (2001), 289-335.

[39] K. Xu, Discontinous Galerkin BGK method for viscous flow equations: one-dimensional systems, *SIAM J. Sci. Comput*, **25** (2004), 1941-1963.

[40] J.Y. Yang, T.Y. Hsieh, Y. Shi and K. Xu, High-order kinetic flux vector splitting schemes in general coordinates for ideal quantum gas dynamics, *J. Comput. Phys.*, **227** (2007), 967-982.